

Galerkin model for time super-sampling of PIV measurements

Qihong L. Li-Hu*, Patricia García-Caspueñas, Andrea Ianiro, Stefano Discetti

Dept. of Aerospace Engineering, Universidad Carlos III de Madrid, Spain

*Corresponding author: qihonglorena.li@uc3m.es

Keywords: PIV, Galerkin model, POD, Jet flow, Time super-sampling.

ABSTRACT

We propose a data-driven method for increasing the time resolution of snapshot Particle Image Velocimetry. The flow dynamics are reconstructed by integrating in time an empirical Galerkin model based on Proper Orthogonal Decomposition modes of the flow field, as developed by Noack et al. (2005). The main objective is to obtain a time-resolved description of the flow dynamics of an experimental non-time-resolved dataset. The proposed methodology is assessed both with numerical and experimental data of a wake and a jet flow. The results we obtained indicate that the method can effectively reconstruct the flow dynamics over a duration spanning several flow characteristic times.

1. Introduction

Time-resolved (TR) Particle Image Velocimetry (PIV) is an important and valuable tool for capturing complete details about the dynamics of turbulent flows. The information about the flow dynamics is of special relevance for flow control purposes. However, the cost of equipment and technological barriers, such as the maximum sampling rate of cameras, the pulsation frequency of light sources, and the lowest signal/noise ratio due to the limited laser-pulse intensity and camera sensitivity, restrict the availability of TR measurements to low-to-moderate Reynolds number flows. Therefore, it is appealing to develop methodologies to increase the time resolution of snapshot PIV for cases where TR PIV is not feasible.

Turbulent flows exhibit inherent patterns whose dynamics often evolve on low-dimensional attractors. Thus, by selecting a proper basis, it is possible to develop condensed models that enable time-marching estimations to represent the main dynamical features of the flow. This strategy has been followed in the recent past by exploiting physical constraints, such as Taylor's hypothesis (de Kat & Ganapathisubramani (2012); Scarano & Moore (2012)) or advection of vorticity (Schneiders et al. (2016)). However, one of the primary limitations of these approaches is the validity of the hypothesis upon which they are based. In particular, Taylor's hypothesis is highly contingent on the selection of an appropriate convection velocity, and its efficacy is severely limited in three-dimensional and/or evolving flows.

In this work, we integrate a Galerkin model based on empirical eigenfuncions to obtain a time super-sampling of non-time-resolved (NTR) velocity fields that can be obtained from PIV experiments. We leverage the Galerkin model proposed by Noack et al. (2005) to obtain reduced-order flow dynamics. Proper Orthogonal Decomposition (POD, Berkooz et al., 1993) modes are used as empirical eigenfuncions, and the NTR instantaneous velocity fields are used as initial conditions to obtain a temporal sequence. Note that this method can be used for either short-term predictions or time super-sampling of subsequent snapshots.

The mathematical background is detailed in §2. Section 3 reports the validations of the Galerkin model employing two subsampled datasets: a DNS dataset of the wake of a fluidic pinball and a dataset of TR PIV measurements of a turbulent jet.

2. Methodology

Through the projection of the Navier-Stokes equations onto an orthonormal basis, the Galerkin method transforms a set of partial differential equations into a set of ordinary differential equations. In this context, the empirical Galerkin model proposed by Noack et al. (2005) is based on the projection of the incompressible Navier-Stokes equations onto a domain spanned by an orthonormal basis obtained through a POD of the velocity fields ($\mathbf{u}(\mathbf{x}, t)$) in terms of spatial modes φ_i :

$$\mathbf{u}(\mathbf{x}, t) := \sum_{i=0}^{\infty} \mathbf{a}_i(t) \varphi_i(\mathbf{x}), \quad (1)$$

where \mathbf{x} and t are respectively the spatial and temporal coordinates, \mathbf{a}_i are the temporal coefficients and φ_i the spatial modes. Note that index 0 refers to the time-averaged velocity field such that $\varphi_0 = \frac{\langle \mathbf{u} \rangle}{|\langle \mathbf{u} \rangle|}$ and $a_0 = |\langle \mathbf{u} \rangle|$, and $\mathbf{a}_i := (\mathbf{u} - \langle \mathbf{u} \rangle, \varphi_i)_{\Omega}^*$.

POD minimizes the Frobenius norm of the residual energy of the data set, i.e. the projection onto the corresponding subspace retrieves the maximum possible energy for a given number of modes. Numerically, this is computed with a Singular Value Decomposition (SVD) following the snapshot method of Sirovich (1987), where the snapshot matrix is $\mathbf{U} \in \mathbb{R}^{N_p \times N_t}$, N_p is the number of spatial points times the vector field dimension and N_t the total number of snapshots without temporal resolution. Typically, $N_p \gg N_t$, so the economy-size SVD of the snapshot matrix is computed as follows:

$$\mathbf{U}(\mathbf{x}, t) = \mathbf{\Phi}(\mathbf{x}) \mathbf{\Sigma} \mathbf{\Psi}^*(t), \quad (2)$$

* $(\mathbf{v}, \mathbf{w})_{\Omega} = \int_{\Omega} dV \mathbf{v} \cdot \mathbf{w}$, inner product in the space of square-integrable vector fields on the domain Ω .

where $\Phi \in \mathbb{R}^{N_p \times N_t}$ and $\Psi^{N_t \times N_t}$ are unitary matrices containing the spatial and temporal modes respectively, and $\Sigma \in \mathbb{R}^{N_t \times N_t}$ is a diagonal matrix containing the singular values σ_i sorted from larger to smaller. The square of the singular values σ_i^2 is representative of the contribution of each mode to the variance of the flow. Here, $*$ denotes the complex conjugate transpose. Then, from Eq. 1-2 the POD temporal coefficients can be retrieved $\mathbf{A} = \Sigma\Psi^*$.

The evolution equation for the expansion coefficients \mathbf{a}_i in the Galerkin approximation is derived by projecting the incompressible Navier-Stokes equation onto the N -rank POD basis. This process, known as the Galerkin projection, results in the following system of equations:

$$\frac{d}{dt}\mathbf{a}_i = \frac{1}{Re} \sum_{j=0}^N l_{ij}\mathbf{a}_j + \sum_{j=0}^N \sum_{k=0}^N q_{ijk}\mathbf{a}_j\mathbf{a}_k + \mathbf{f}_i^\pi(\mathbf{A}) \quad \text{for } i = 1, \dots, N, \quad (3)$$

where $l_{ij} := (\varphi_i, \Delta\varphi_j)_\Omega$ and $q_{ijk} := (\varphi_i, \nabla \cdot (\varphi_j\varphi_k))_\Omega$ are the coefficients of the viscous and convective terms. $\mathbf{f}_i^\pi := -(\varphi_i, \nabla p)_\Omega$ is the pressure term. It shall be noted that we are parting from the assumption of NTR snapshot PIV, where the obtention of pressure field measurements is elusive. Thus, our proposed Galerkin model for the tackled flow configurations neglects the pressure contribution and solely considers the terms of the dynamical system that depend on velocity.

Flow super-sampling of poorly-resolved datasets can be done by time-marching methods where the velocity fields between available snapshots are reconstructed by integrating the evolution equation Eq. 3 in time. For simplicity, we choose a time-step equal to the TR Δt of the reference dataset, with the given snapshots as the initial conditions of the integration. However, this reconstruction of the flow dynamics around the snapshots is limited, as it is highly dependent on the time separation between the snapshots. A large separation implies that the error propagation in the integration is more severe. Therefore, the following strategy is considered. The evolution equation is integrated forward and backward in time up to the midpoint of two consecutive snapshots, where the average between both results is computed. Then, a second integration is done from the midpoint towards the known initial and final snapshots performing backward and forward integration, respectively. At the midpoint, the initial condition of the integration is updated with the average value between the first integration. Then, the initial conditions of the second integration phase are updated with a weighted average between the solution of the first integration phase and the solution of the previous step in the second integration. Since the initial and final snapshots are known, the idea of this correction is to add information from the final and initial conditions respectively.

3. Validation

The method is evaluated on two different datasets, the first obtained from a DNS of a fluidic pin-ball, and the second from experimental data of a water jet flow.

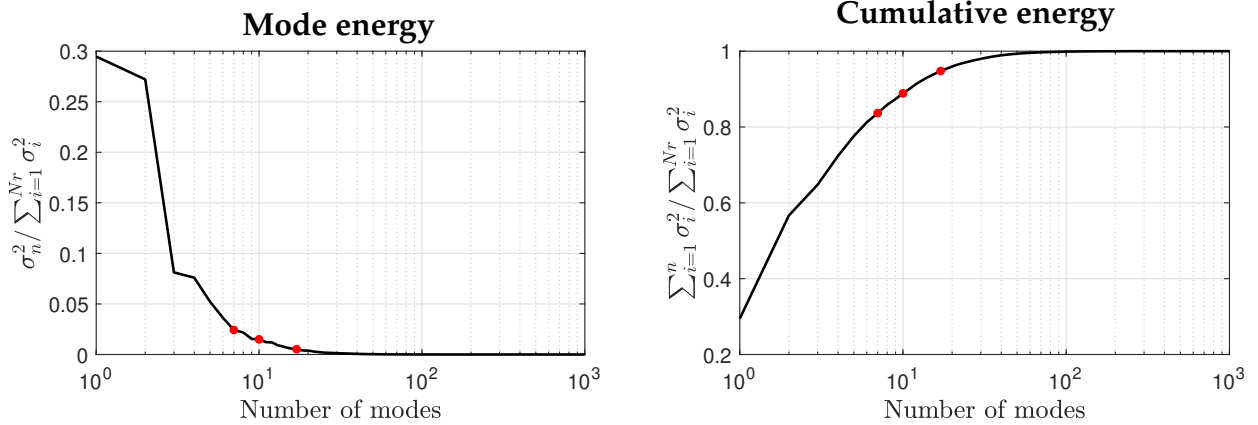


Figure 1. Energy and cumulative energy distribution (left and right) for increasing number of modes of the fluidic pinball. In red dots the rank truncations used for the analysis (respectively 85%, 90% and 95% of the total energy).

The performance of the model is significantly affected by two main factors, the number of modes chosen to truncate the reconstruction and the time separation between snapshots. The effect of rank truncation, where the number of modes is reduced to simplify the model, is critical as it determines the total energy of the flow that can be reconstructed. The time separation between snapshots affects the accuracy of the temporal integration, as integration errors propagate and amplify with time, especially in the case of widely spaced snapshots potentially leading to inaccuracies and integration blow-up in the reconstructed flow fields.

To test the robustness of the model, different rank truncations as well as temporal separations between snapshots are explored.

3.1. Fluidic pinball

A synthetic dataset obtained from a 2D DNS of the wake behind a fluidic pinball (Deng et al. (2020)) is used as a benchmark for validating the Galerkin model in time-supersampling applications. This simulation features three cylinders, each with a diameter D , arranged in an equilateral triangle with side lengths of $3D/2$. The configuration is immersed in a flow with uniform velocity U_∞ .

The simulation is performed at a Reynolds number $Re = 130$, which places it in the symmetric chaotic regime (Deng et al. (2020)). Velocity, acceleration and pressure data are interpolated on a Cartesian grid, where $\tilde{x} = x/D \in [-5, 15]$ and $\tilde{y} = y/D \in [-5, 5]$, with a constant grid spacing of $d\tilde{x} = d\tilde{y} = 0.1$. The time step for the DNS is $d\tilde{t} = 0.1$ with $\tilde{t} = tD/U_\infty$, which is the time normalized by the convective time. Finally, the time-resolved snapshots obtained from the DNS are downsampled into a sequence of NTR measurements of velocity.

The data set consisting of unresolved 2D velocity fields is used to estimate the coefficients of the Galerkin model. Therefore, the original data set containing 10000 snapshots is downsampled by S_r number of snapshots. Two different cases are considered, the first one with a time spacing of

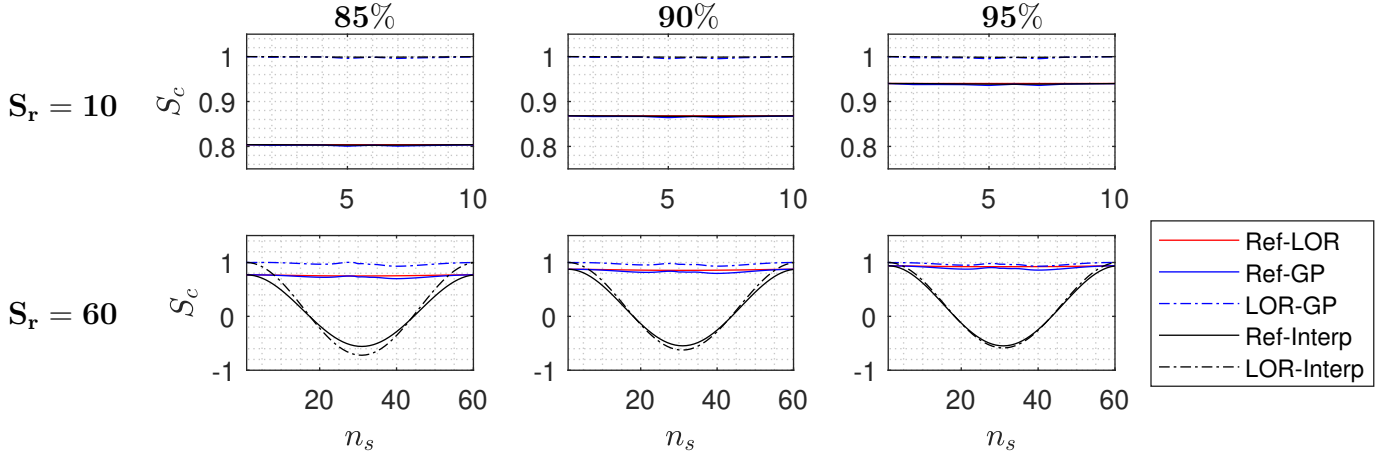


Figure 2. Mean cosine similarity (S_c) between estimated and reference fluctuation velocity fields for varying temporal spacing from the initial conditions. The top row indicates a sub-sampling rate of 10 snapshots (i.e. 1 convective time), while the bottom row has a sub-sampling rate of 60 snapshots (i.e. 6 convective times). Red, black, and blue lines respectively denote the LOR, cubic-spline, and Galerkin comparison with respect to the reference case. Absolute error against the reference fields are represented by solid lines, whereas relative errors to the LOR are indicated with dashed ones.

$\tilde{t} = 1$, taking one snapshot every $S_r = 10$, and the second one with a time separation of $\tilde{t} = 6$ taking a snapshot every $S_r = 60$. For each of them, three different low-order reconstructions (LOR) have been selected in terms of the total reconstructed energy, namely, 85%, 90%, and 95%.

As it can be observed in Fig. 1, the number of modes to which the reconstructions are truncated is close to the elbow of the mode energy plot, therefore, the number of modes required for these levels of energy does not vary largely between them as will happen later with the turbulent jet flow.

The velocity fields reconstructed with the Galerkin model (GP) are compared to the reference snapshot from the TR PIV, the Low-Order Reconstruction (LOR) with the same number of modes (which is theoretically the best reconstruction that can be achieved by the LOR), and the reconstruction with temporal modes interpolated with a cubic-spline between time instants where data is available (Interp). Since only a certain percentage of the total energy is reconstructed, the final velocity fields will include the truncation error introduced by the LOR. Consequently, a comparison between the GP and the LOR provides insight into the additional error introduced by the integration of the Galerkin model itself.

The cosine similarity (S_c) between the velocity fields is calculated as a function of the time separation relative to the snapshots in the dataset. Fig. 2 illustrates that for a small sub-sampling rate (S_r), both reconstructions closely match the reference. For separation of only 1 convective time ($S_r = 10$) Interp and GP perform similarly. However, for snapshots separated by several convective times, the reconstruction using interpolated modes begins to fail. Visual inspection of the animated sequence also exhibits unphysical dynamical behaviour. In contrast, the GP maintains

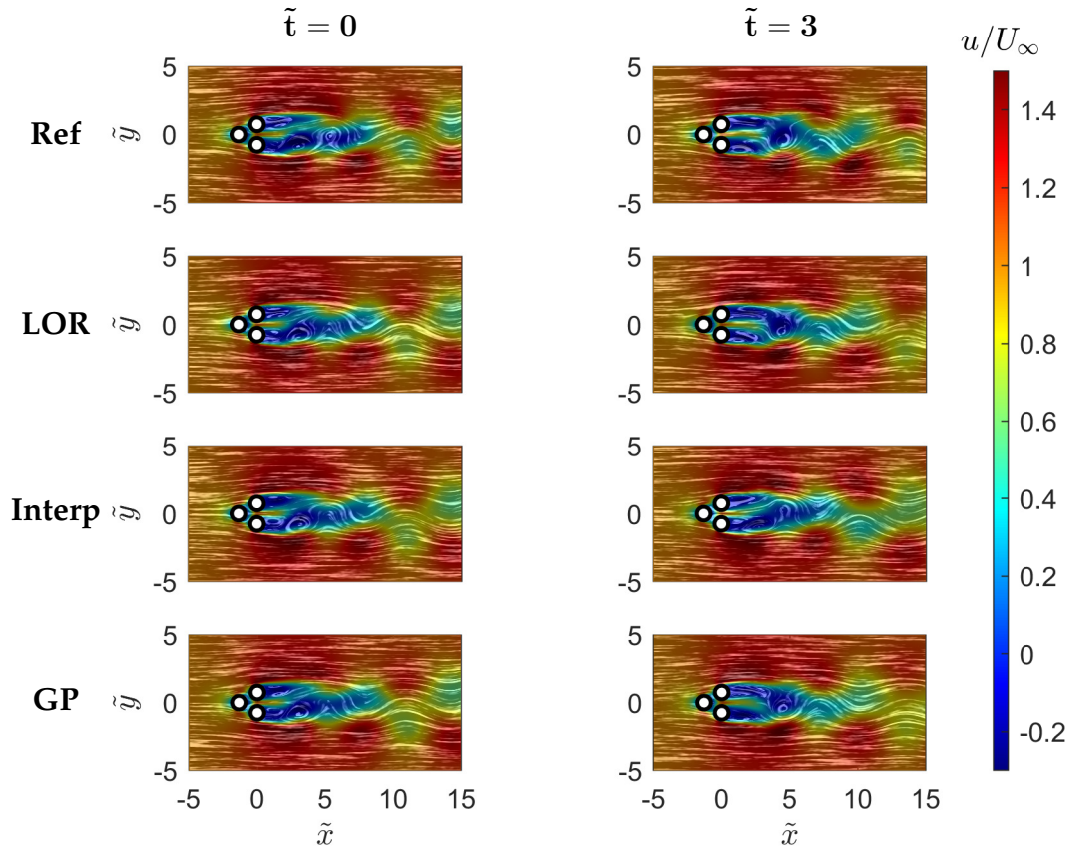


Figure 3. Reconstruction with 90% of the total energy of streamwise velocity fluctuations of in-sample snapshots of the $S_r = 60$ subsample dataset. Left: snapshot at the initial instant. Right: reconstructed snapshot positioned midway between two consecutive snapshots from the subsampled sequence. From top to bottom: reference field, LOR, interpolated reconstruction, and Galerkin model results.

good reconstructions. Furthermore, the results are compared in terms of energy reconstruction in order to assess the impact of the truncation error in the results. As illustrated in Fig. 2, the similarity coefficient increases with the total energy, thereby reducing the truncation error.

$$S_c = \frac{\mathbf{u}'_{\text{ref}} \cdot \mathbf{u}'_{\text{recon}}}{\|\mathbf{u}'_{\text{ref}}\|^2}, \quad (4)$$

where $\mathbf{u}' = \mathbf{u} - \langle \mathbf{u} \rangle$, and subscript recon refers to the estimated fields, both with the Galerkin model or with interpolation.

Fig. 3 shows the streamwise velocity fields reconstructed with 90% of total energy without adding the pressure coefficient terms at two different time instants. The first column depicts a snapshot from the specified NTR dataset while the second column illustrates a snapshot taken equidistantly between two consecutive available snapshots for the case of $S_r = 60$, where the error is statistically maximum. The direct interpolation of POD modes does not identify correctly the phase of the shedding, most likely due to aliasing of the heavily downsampled sequence of modes. On the

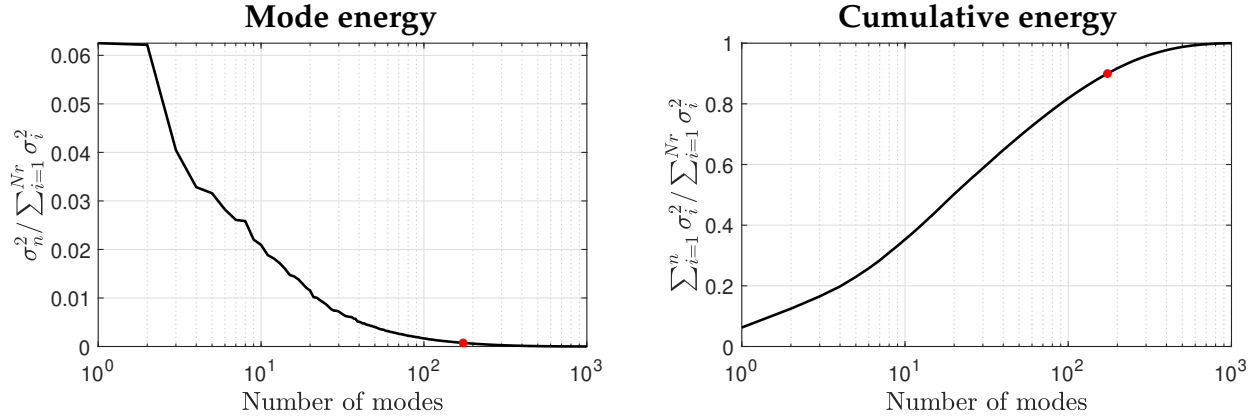


Figure 5. Energy and cumulative energy distribution (left and right) for increasing number of modes of the fluidic pinball. In red dots, the rank truncation used for the analysis, corresponding to 90% of the energy.

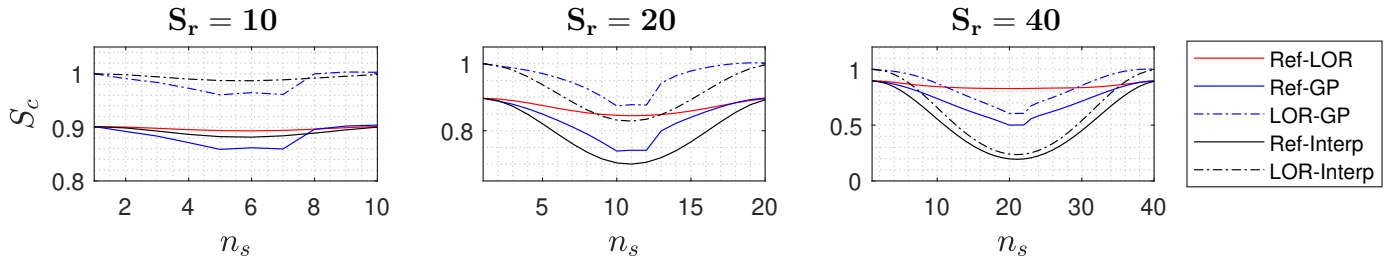


Figure 6. Mean cosine similarity (S_c) between estimated and reference fluctuation velocity fields for varying temporal spacing from the initial conditions. Red, black, and blue lines respectively denote the LOR, cubic-spline, and Galerkin comparison with respect to the reference case. Absolute error against the reference fields are represented by solid lines, whereas relative errors to the LOR are indicated with dashed ones.

Subsequently, the post-processed images are low-pass filtered with a Savitzky-Golay filter, comprising a 5-snapshots kernel in time and a 5×5 grid point kernel in space. A Gaussian filter is applied to enhance the smoothing of temporal data.

The flow dynamics are reconstructed for three different sub-sampling ratios, with a total energy of 90% (Fig. 5). In contrast to the prior validation case, the jet flow requires a greater number of modes to reconstruct the main flow features (see Fig. 5). Differently from before, achieving a higher percentage of energy demands a large number of modes, which consequently leads to a rapid increase in the computational time. Therefore, for simplicity, only one energy level is selected for the reconstruction and the comparison focuses on the effect of the sub-sampling ratio.

Three different sub-sampling ratios are evaluated, namely $S_r = 10$, $S_r = 20$, and $S_r = 40$ (corresponding to $\tilde{t} = 0.4$, $\tilde{t} = 0.8$ and $\tilde{t} = 1.6$ respectively). Comparing the values of the cosine similarity for all the cases (Fig.6), it is observed that for small downsampling factors, the reconstruction with the interpolation seems to perform slightly better than the Galerkin model. On the other hand, when increasing the sub-sampling ratio, the Galerkin model performs better since the interpolation is affected by a too-low Nyquist frequency. This can be observed in Fig. 7 and 8, where the interpolated fields at the midpoint between consecutive snapshots exhibit greater discrepancies

from the reference snapshot as compared to the Galerkin model.

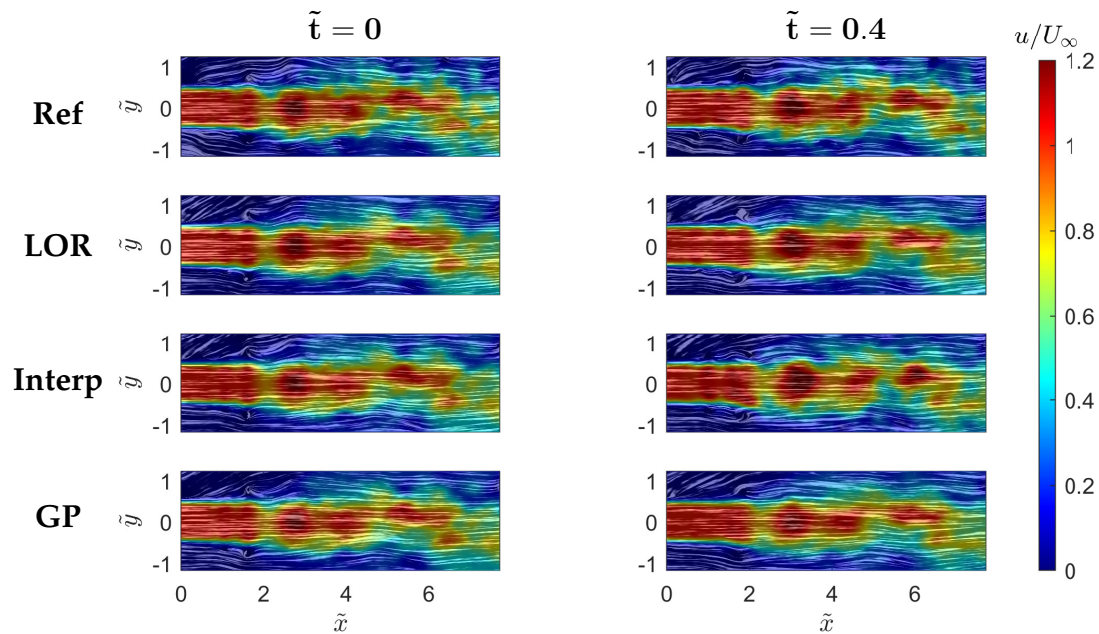


Figure 7. Reconstruction with 90% of the total energy of streamwise velocity fluctuation contours of an in-sample snapshot of the $S_r = 20$ subsample dataset. On the left: the snapshot used as the initial condition. On the right: the reconstructed snapshot positioned midway between two consecutive snapshots from the subsampled sequence.

From top to bottom: reference field, LOR, interpolated reconstruction, and Galerkin model results.

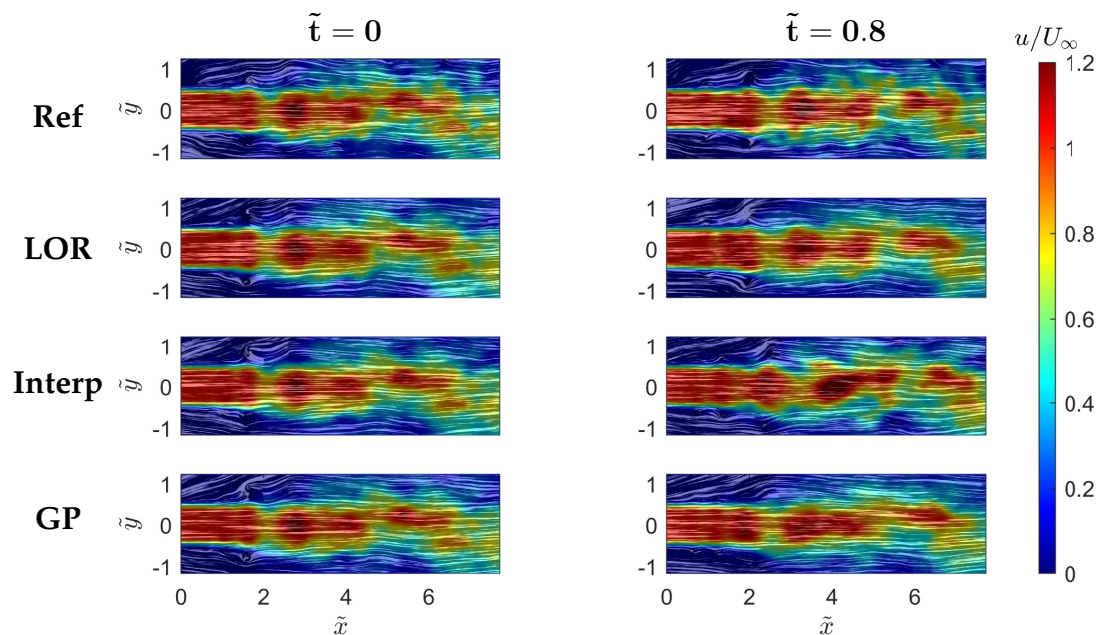


Figure 8. Reconstruction with 90% of the total energy of streamwise velocity fluctuation contours of an in-sample snapshot of the $S_r = 40$ subsample dataset. On the left: the snapshot used as the initial condition. On the right: the reconstructed snapshot positioned midway between two consecutive snapshots from the subsampled sequence.

From top to bottom: reference field, LOR, interpolated reconstruction, and Galerkin model results.

4. Conclusion

A dynamic model based on Galerkin projection has been proposed for the temporal supersampling of consecutive non-time-resolved PIV measurements, where only velocity fields are available. The objective of this model is to enhance temporal resolution and reconstruct flow dynamics, thereby providing a more detailed and continuous representation.

The reconstruction quality depends on the number of modes considered in the low-order model. Our results show that the GP model consistently improves when increasing the number of modes involved in the model, although the computational cost of the integration might become a concern.

Additionally, the model was compared to a reconstruction using interpolated temporal coefficients at different sub-sampling rates with respect to the ideal time resolution required to describe the flow in a hypothetical TR PIV experiment. It was observed that for small time separation, typically less than one convective time depending on flow complexity, direct interpolation of the POD modes yielded superior results to those obtained using the Galerkin model. Nevertheless, for larger time separations, interpolation is unable to resolve the reconstructed coefficients due to aliasing, whereas the Galerkin model performs more effectively.

The Galerkin model has been found to be an effective means of reconstructing the dynamics of turbulent flows from NTR velocity fields that are separated by several convective times. When the flow evolves rapidly, with dynamics depending on small-scale structures, the reconstruction's accuracy is significantly dependent on the total energy captured, as missing information can lead to fast-propagating errors. Further work will be done to evaluate the influence of the pressure term and to smooth the evolution of the reconstructed time-resolved velocity fields.

5. Acknowledgement

This project has received funding from the European Research Council (ERC) under the European Union's Horizon 2020 research and innovation program (grant agreement No 949085). Views and opinions expressed are however those of the authors only and do not necessarily reflect those of the European Union or the European Research Council. Neither the European Union nor the granting authority can be held responsible for them. The jet experiment presented herein was designed by Mr. Luca Franceschelli. We kindly thank him for granting the availability of the experimental setup to collect the dataset for the experimental validation of our method.

References

Astarita, T. (2006). Analysis of interpolation schemes for image deformation methods in piv.

Experiments in fluids, 40, 977–987.

Astarita, T., & Cardone, G. (2005). Analysis of interpolation schemes for image deformation methods in piv. *Experiments in fluids*, 38, 233–243.

Berkooz, G., Holmes, P., & Lumley, J. L. (1993). The proper orthogonal decomposition in the analysis of turbulent flows. *Annual Review of Fluid Mechanics*, 25(1), 539–575. doi: 10.1146/annurev.fl.25.010193.002543

de Kat, R., & Ganapathisubramani, B. (2012). Pressure from particle image velocimetry for convective flows: a Taylor's hypothesis approach. *Measurement Science and Technology*, 24(2), 024002.

Deng, N., Noack, B. R., Morzyński, M., & Pastur, L. R. (2020). Low-order model for successive bifurcations of the fluidic pinball. *Journal of Fluid Mechanics*, 884, A37. doi: 10.1017/jfm.2019.959

Noack, B. R., Papas, P., & Monkewitz, P. A. (2005). The need for a pressure-term representation in empirical Galerkin models of incompressible shear flows. *Journal of Fluid Mechanics*, 523, 339–365. doi: 10.1017/S0022112004002149

Paolillo, G., & Astarita, T. (2024, July 08–11). Pairs-unina: A robust and accurate free tool for digital particle image velocimetry and optical camera calibration. In *Proceedings of 21st international symposium on applications of laser and imaging techniques to fluid mechanics*. Lisbon, Portugal.

Scarano, F., & Moore, P. (2012). An advection-based model to increase the temporal resolution of piv time series. *Experiments in fluids*, 52, 919–933.

Schneiders, J. F. G., Pröbsting, S., Dwight, R. P., van Oudheusden, B. W., & Scarano, F. (2016). Full-field pressure from snapshot and time-resolved volumetric PIV. *Experiments in Fluids*, 53(4).

Sirovich, L. (1987). Turbulence and the dynamics of coherent structures. i, ii, iii. *Quarterly of applied mathematics*, 45(3), 561–590.